Food Hydrocolloids 134 (2023) 108059

Contents lists available at ScienceDirect

Food Hydrocolloids

journal homepage: www.elsevier.com/locate/foodhyd

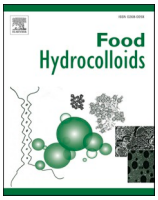

Effect of L-cysteine and L-ascorbic acid addition on properties of meat analogues

Somayeh Taghian Dinani *, Jeroen Philip van der Harst, Remko Boom, Atze Jan van der Goot **

Food Process Engineering, Wageningen University & Research, PO Box 17, 6700 AA, Wageningen, the Netherlands

ARTICLE INFO

Keywords:
L-cysteine
L-ascorbic acid
Pea protein isolate
Plant-based meat alternatives
Fibrous structure

ABSTRACT

Currently, studies are underway to use pea protein isolate (PPI) for the production of meat analogues because it is considered as a more sustainable alternative to soy. The potential of PPI has been demonstrated in extrusion and PPI in combination with wheat gluten has been studied in the shear cell. To enlarge the possibilities to make meat analogues with a broader range of properties, the effects of L-cysteine (CYS) and L-ascorbic acid (AA) on PPI and wheat gluten (WG) blends were examined at different concentrations (0, 100, 500, 1000 and 2000 ppm). The results showed that both CYS and AA altered the properties of the products formed by the high-temperature shear cell (HTSC). Both additives altered the fibrousness and the mechanical properties of the products obtained after processing. Especially CYS revealed an increase in tensile stress, tensile strain and Young's modulus as its concentration increased. However, products containing CYS depicted a relatively stable anisotropic index of 1, which corresponded to a densely packed matrix that was observed by microstructural analysis. A small elevated anisotropic index (>1) of products containing AA at concentrations of 500–2000 ppm could be attributed to the formation of pores parallel to the shear flow direction in these samples visualized by a confocal laser scanning microscope (CLSM) and the scanning electron microscope (SEM). In the products containing 2000 ppm of AA and 2000 ppm CYS, small and large fibers were formed, respectively. Therefore, this research pointed out the potential application of CYS and AA to alter and control the textural attributes of products. This application could aid in improving the consumer acceptance of meat analogues and, thus, contribute to being able to feed the increasing population of the world.

1. Introduction

There is a strong societal trend toward reduction of meat consumption (Michel, Hartmann, & Siegrist, 2021). However, so far only a limited population has shifted towards consuming meat analogues (Hoek et al., 2011; Kendler, Duchardt, Karbstein, & Emin, 2021; Stiftung, Böll, & Terre, 2014) mostly because these still deviate from meat in terms of texture, mouthfeel, taste, flavor and nutritional attributes (Hoek et al., 2011).

Today, soy protein concentrates and isolates (SPI) are common and mostly used with wheat gluten (WG) in meat analogues produced especially, by extrusion process due to their favorable gelation properties (Banerjee & Bhattacharya, 2012; Day & Swanson, 2013) and creation of an interlaced, fibrous matrix (Schreuders et al., 2019). However, soy is allergenic and connected to GMO concerns (Gizzarelli et al., 2006). Therefore, pea protein isolate (PPI) is suggested to be a better protein resource for these foods (Schreuders et al., 2019), and, thus, is widely used now. Moreover, as soy is mainly produced in South American countries, transport for the European market negatively affects the environment. Furthermore, soil erosion and intense logging in rain forests (Brazilian Amazonia) to free up land for soy cultivation, also negatively impacts the environment in terms of loss of biodiversity (Davis, Sonesson, Baumgartner, & Nemecek, 2010; Thrane, Paulsen, Orcutt, & Krieger, 2017). Pea can be harvested in Europe, which could improve transport emissions (Davis et al., 2010). Besides, Cederberg and Flysjö (2004) found that products that are produced more regionally have advantages in resource use, climate change, eutrophication, and land use. Therefore, the application of peas instead of soy could be a good alternative to produce meat analogues (Davis et al., 2010) and nowadays, pea protein is a common ingredient. Regarding the fact that producing anisotropic fibrous structures in a shear cell requires two phases and PPI itself cannot produce anisotropic fibrous structures, WG

* Corresponding author.
** Corresponding author.
E-mail addresses: somayeh.taghiandinani@wur.nl (S. Taghian Dinani), atzejan.vandergoot@wur.nl (A.J. van der Goot).

https://doi.org/10.1016/j.foodhyd.2022.108059
Received 31 May 2022; Received in revised form 2 August 2022; Accepted 7 August 2022
Available online 11 August 2022

is mostly used with PPI (Grabowska, Zhu, Dekkers, Ruijter, et al., 2016).

However, PPI forms weaker gels (Schreuders et al., 2019; Shand, Ya, Pietrasik, & Wanasundara, 2007) and has lower gelling capacity (Bildstein, Lohmann, Hennigs, Krause, & Hilz, 2008) compared to SPI. In fact, soybean glycinin can produce a better-structured gel network than pea legumin due to the formation of more-organized strands (O'kane, Happe, Vereijken, Gruppen, & Boekel, 2004). It is therefore interesting to better understand the differences and explore routes to bridge the gap (Banerjee & Bhattacharya, 2012; Day & Swanson, 2013; Peng et al., 2022; Schreuders et al., 2019). To achieve this target, adding some additives, in particular, oxidizing/reducing agents could enhance the favorable fibrous structures. In fact, these agents are usually used to change the sulfhydryl (SH)/disulfide (S–S) interchanges of proteins and physical properties of final products (Mei Li & Lee, 1998). In this study, L-cysteine (CYS) and L-ascorbic acid (AA) were tested based on their effect on the structural properties of protein blends. Both CYS and AA are accepted food additives, which are added to bread flour or dough for improving the quality of dough, bread and extrudates (Majzoobi, Farahnaky, Jamalian, & Radi, 2011).

CYS is a sulfur-containing amino acid whose redox potential is close to that of the S–S bonds in proteins and thus could reduce the S–S groups. This will affect the network structure of macromolecules and protein aggregation during processing (Mei Li & Lee, 1998; Peng et al., 2022; Takagi & Ohtsu, 2017; Wiedemann, Kumar, Lang, & Ohlenschläger, 2020). Pulse proteins are usually deficient in CYS amino acid (Boye, Zare, & Pletch, 2010) and addition of CYS could significantly and differently alter the physical, microstructural, and functional properties of products (Mei Li & Lee, 1998). Lambert and Kokini (2001) reported that the properties of wheat flour extrudates treated with different concentrations of CYS were inconsistent (Lambert & Kokini, 2001). In other studies, varying results were also reported. For instance, Li and Lee (1996) investigated the effect of added CYS from 0 to 1.5% (15000 ppm) on the functional and microstructural properties of wheat flour extrudates, and suggested that CYS affects the gluten in two ways: 1. breaking the interchain S–S bonds and, thus, reducing the gluten molecular weight. 2. hindering the S–S bond polymerization in gluten, and, thus, reducing the network formation and producing a weakened network. Contrary to this hypothesis, they reported that increasing the concentration of CYS could almost double the S–S content and it decreased the number of free SH groups linearly in the extrudate. Moreover, the results of this study showed that increasing CYS concentration increased the cohesiveness and gumminess and decreased the water-holding capacity of the extrudates (Li & Lee, 1996).

In the next study, Li and Lee (1998) reported that increasing the CYS concentration led to a decrease in the molecular size of the cross-linked wheat proteins and, thus, an increase in their solubility. In this study, they reported that the interchange between added CYS and the S–S bonds of the protein led to the weakening of the disulfide-mediated cross-linking inside the wheat proteins. In addition, an increased SH content and higher protein solubility were found (Mei Li & Lee, 1998). In another study, Riha, Hwang, Karwe, Hartman, and Ho (1996) reported that increasing the CYS concentration from 0 to 10,000 ppm increased dough strength evidenced by the fact that the specific mechanical energy of the final extruded product increased from 452 to 752 kJ/kg, respectively. In a recent paper, Peng et al. (2022) reported that the addition of CYS decreased the SH group content of extruded pea protein isolate because of an oxidation reaction and S–S bond formation during extrusion. They found a dense structure and a significant increase in hardness of extrudates by increasing the concentration of CYS from 300 to 900 ppm but then reducing hardness from 900 ppm to 1500 ppm CYS. Therefore, inconsistent and different results have been reported regarding the effect of CYS on different protein resources used in different papers.

AA is the main oxidizing agent to improve bread quality mainly from weak flour (with low protein content especially less gluten) without health restrictions (Stoica, Bărăscu, & Iuja, 2013). It can be oxidized into dehydroascorbic acid (DHAA) in the presence of oxygen (Dale Every, Motoi, Rao, Shorter, & Simmons, 2008), which acts as an oxidizing agent resulting in a decrease in SH bonds and an increase in S–S bond formation. This formation of S–S bonds in between protein molecules improves the flour's physicochemical and baking properties (Lu & Seib, 1998). Again, although the influence of AA was tested on dough and bread made with wheat flour (Hruskova, Novotna, Hrušková, & Novotná, 2003; Joye, Lagrain, & Delcour, 2009; Lu & Seib, 1998; Stoica et al., 2013), it has not yet been tested on meat analogue production using PPI-WG blends in the high-temperature shear cell (HTSC).

HTSC uses high temperature and shear flow to create a fibrous structure, like high moisture extrusion. However, the aforementioned parameters with HTSC can be controlled and optimized better to obtain the desired fibrous and anisotropic structures (Manski, van der Goot, & Boom, 2007). Moreover, HTSC uses milder process conditions for product structure formation because of lower applied shear forces and, thus, has a lower energy input. Lower energy input facilitates the scale-up of this system in the near future and thus, this device can be used both on small (retail) and larger (factory) scales (Grabowska, Zhu, Dekkers, De Ruijter et al., 2016). In HTSC, the shearing zone is created between the surfaces of two cones, the rotating bottom cone and the stationary top cone. In fact, the shear cell's cone-in-cone angular design provides a constant and homogeneous linear shear throughout the cell because of the small gap between cones (Merkel, Emin, Schuch, & Schuchmann, 2015). The processing steps in HTSC generally consist of three processing steps: a mixing step, followed by a thermo-mechanical treatment and lastly a cooling step (Fig. 1. A).

This exploratory research is aimed at investigating the influence of CYS and AA in various concentrations (0, 100, 500, 1000 and 2000 ppm) on PPI-WG blends processed in the HTSC. The possibilities to alter fiber formation, color and textural properties were quantified. As these additives are used successfully in dough and bread preparation to change the protein network in the proteins and to improve the quality of final products, it is hypothesized that these additives could have a favorable impact on the textural properties of the protein blends resulting in a more fibrous structure and strength after HTSC processing. Moreover, it is believed that different concentrations of these additives correspond with different textural and sensorial characteristics of the meat analogues formed.

2. Materials and methods

2.1. Materials

Pea protein isolate (PPI) (NATURALYS© S85F) and vital wheat gluten (WG) (VITENS© CWS) were obtained from Roquette Freres S.A. (Lestrem, France). PPI (with a dry matter content of 92.6%) and WG (with a dry matter content of 92.0%) were composed of 78.6% (N x 5.7) and 72.4% (N x 5.7) protein on a dry basis, respectively, according to Dumas measurements. Furthermore, CYS (97.0%) and AA (≥98.0%) were bought from Sigma-Aldrich co., LCC (Zwijndrecht, the Netherlands). Rhodamine B was purchased from Sigma-Aldrich Chemie Gmbh (Steinheim, Germany) and used as a staining agent for confocal laser scanning microscope (CLSM) analysis. Finally, glutaraldehyde, ethanol and carbon cement glue were obtained from Sigma-Aldrich (Steinheim, Germany), VWR International (Strasbourg, France) and Plano GmbH (Wetzlar, Germany) companies, respectively, and were used for the scanning electron microscope (SEM) analysis. All reagents and chemicals used in this study were of analytical grade.

2.2. Methods

2.2.1. Preparation of protein mixtures

All products were prepared by mixing 40 wt% ingredients and 60 wt % deionized water. The ingredients mix consisted of 50 wt% PPI and 50 wt% WG (Schreuders et al., 2019). In the case of additive addition, the

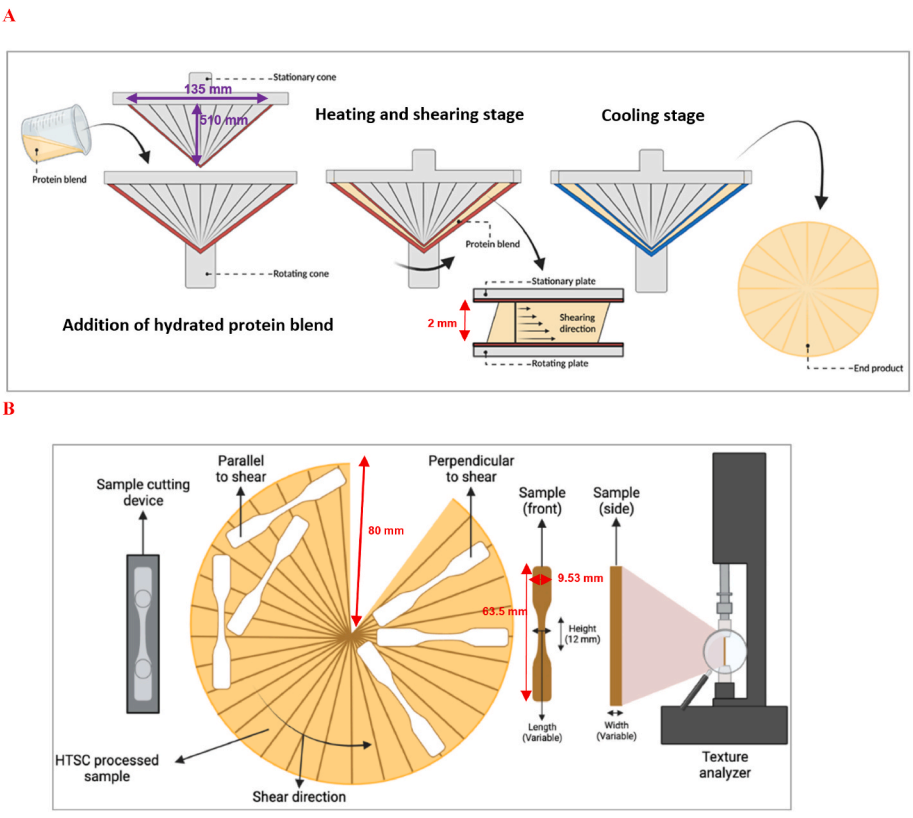

Fig. 1. **A:** Schematic overview of the operation of the HTSC when shearing a hydrated protein blend. The protein blend is added to the heated shear cell (indicated with the red lines in the shear cell). The HTSC starts to operate by heating at a constant temperature and rotating (shearing) at a constant rate. After the heating and shearing stage, the HTSC is cooled down (indicated with blue in the shear cell) without rotation after which a sheared material (final product) is obtained. **B:** Schematic overview of the tensile strength analysis for meant analogues after processing by HTSC. (For interpretation of the references to color in this figure legend, the reader is referred to the Web version of this article.)

water content was lowered accordingly (Table 1). To prepare products, first, CYS or AA at the desired concentration (100, 500, 1000 and 2000 ppm) was dissolved in deionized water followed by the addition of 20% PPI. For the control, PPI was directly added to deionized water as this sample contains no CYS or AA in its formulation (Table 1). The mixture was then manually stirred using a spatula until it was completely mixed. The obtained protein mixture was covered with parafilm and left to hydrate at room temperature for 30 min. After hydration, 20% WG was added to compose the final PPI-WG blend. Further mixing with a spatula was done for 1 min and the sample was transferred to the HTSC and processed according to section 2.2.2.

Table 1
Composition of 9 different protein blends investigated in this study. In this table, the abbreviations of CYS, AA, PPI and WG mean L-cysteine, L-ascorbic acid, pea protein isolate and wheat gluten, respectively.

Abbreviations	Treatments	Additive (%)	PPI (%)	WG (%)	Water (%)
C	Control	0	20	20	60
CYS-100	L-cysteine-100 ppm	0.01	20	20	59.99
CYS-500	L-cysteine- 500 ppm	0.05	20	20	59.95
CYS-1000	L-cysteine- 1000 ppm	0.1	20	20	59.9
CYS-2000	L-cysteine- 2000 ppm	0.2	20	20	59.8
AA-100	L-ascorbic acid-100 ppm	0.01	20	20	59.99
AA-500	L-ascorbic acid-500 ppm	0.05	20	20	59.95
AA-1000	L-ascorbic acid-1000 ppm	0.1	20	20	59.9
AA-2000	L-ascorbic acid-2000 ppm	0.2	20	20	59.8

2.2.2. High-temperature shear cell (HTSC) processing of different mixtures

An in-house developed batch HTSC (Wageningen University, the Netherlands) was used to structure 100 g of a protein blend. Simple shear flow was applied to the mixture as the bottom cone of the cone-in-cone geometry rotated while the top cone remained stationary. The cavity (2 mm distance) between the two cones was pressurized (6.5 bar) preventing the escape of steam during processing (Schreuders et al., 2019). The shear rate was conveyed through a Haake™ Polylab™ drive (Haake Polylab QC, Germany) while temperature regulation of the cones was provided by circulating oil through the cones using an oil pump (Thermal H10, JULABO, Germany). A constant rotation speed of 30 rpm (39.1 s^{-1}) at 120 °C for the duration of 15 min was applied, followed by a cooling step of 10 min without any shearing (0 rpm) to 25 °C. After cooling, the top cone was lifted, and the sample was taken out of the shearing device. Then, the sample was kept in an airtight Ziplock bag at room temperature for at least 1 h to prevent moisture loss and to obtain a structurally stable fiber before further analysis (Sha & Xiong, 2020). Visual inspection of the fibrous structure, color measurement and tensile test were performed using freshly made HTSC processed products. After these analyses, the remaining products were frozen at −18 °C in the freezer (Mediline, Liebherr, Germany) for further analysis by CLSM and SEM. All products were made in triplicate unless mentioned otherwise.

2.2.3. Investigation of the fibrous structure

After HTSC processing, the products were folded parallel to the shearing direction and photographed (iPhone SE, Apple, 12 MP) in a photo booth to visualize the fibrous structure formed during processing. The photo booth contained three light-emitting diodes (DV-80SL, Falcon eyes) from 3 different angles (two from each side of the sample and one above it) to ensure similar lighting conditions for every photo.

2.2.4. Color measurement

To measure the L*, a*, and b*color parameters of the freshly processed products, a colorimeter (Konica Minolta inc. Chroma Meter CR-

400, Japan, aperture size 8 mm) was utilized. The color parameters were measured on at least three spots of each replicate. With the measured L*, a* and b* values, the browning index (BI) of each sample were calculated using Eq. (1) (Taghian Dinani & Havet, 2015):

$$BI = \frac{100}{0.17}\left(\frac{(a^{*2} + 1.75L^{*})}{5.645L^{*} + a^{*} - 3.012b^{*}} - 0.31\right) \quad (1)$$

2.2.5. Confocal laser scanning microscopy (CLSM)

CLSM was used to make images on a microscopic level of products containing different concentrations of CYS and AA, to distinguish different components entrapped in the matrix. The CLSM method in this paper was similar to the method described by Schreuders et al. (2019). In more detail, the frozen (−18 °C) HTSC processed samples were cut with dimensions of 5 mm × 8 mm × 10 mm. Next, a cryo-microtome (Micron CR50-H, ADAMAS-instruments Corp., Rhenen, The Netherlands) was utilized to create slices of approximately 40 μm at −20 °C. These were then stained using Rhodamine B (0.1 mg/ml) to visualize the proteins. The confocal laser scanning microscope (Zeiss AG, Oberkochen, Germany) was using a 543 nm HeNe with a 405 nm Blue/Violet diode laser. A 20x EC Plan-Neofluar/0.5 lens was utilized. Finally, the images were analyzed with the help of the blue edition of ZEN software (Carl Zeiss Microscopy). To qualify the high and low-intensity red colors as well as the black color in the CSLM pictures, the color thresholding function in ImageJ software (1.53k National Institutes of Health, USA) was used. The area (%) of black color, high-intensity red color, and low-intensity red color were quantified in each CSLM picture by changing the brightness parameter between 0 and 80, 80–185, and 185–255, respectively, when the total range of brightness is defined from 0 to 255. The default threshold method, red threshold color, and HSB color spacing were selected for all the pictures. For each sample, at least two CSLM pictures were analyzed using this procedure.

2.2.6. Scanning electron microscopy (SEM)

To provide more information on the microstructure of the prepared PPI-WG blends, SEM was performed according to the procedure described by Schreuders et al. (2022). Rectangular pieces (13 mm × 5 mm) were cut from the HTSC processed samples, 1 cm away from the apex. These pieces were put in a glutaraldehyde solution (2.5 v/v%) while gently shaking (Mini Rocker-Shaker MR1, Riga, Latvia) for 8 h. Next, the glutaraldehyde was discarded and replaced by deionized water overnight. Then, the samples were immersed in a series of ethanol solutions for at least 1 h per solution (10, 30, 50, 70, 96 and 100% (v/v)). In the next step, critical point drying (CPD 300, Leica, Vienna, Austria) was performed to dry the samples. The samples were manually fractured parallel to the shear direction, mounted on the stubs using carbon cement glue, and sputter-coated with 12 nm of tungsten (SCD 500, Leica, Vienna, Austria). The surfaces were analyzed with a field emission scanning electron microscope (Magellan 400, FEI, Eindhoven, the Netherlands) at magnifications of 250× (~5 μm) with secondary electron detection using 2.00 kV and 13 pA.

2.2.7. Tensile strength analysis

Tensile strength analysis was performed with a TA. XT plus texture analyzer (Stable Micro Systems Ltd., Surrey, UK) utilizing a static load cell of 50 N at room temperature. A bone-shaped mold was used to cut out pieces of the sample perpendicular and parallel to the shear flow direction (Fig. 1B). The initial height of the bone-shaped pieces of the sample remained constant as the mold had a height of 12 mm. Although the distance between two cones is 2 mm (Fig. 1A), the width of different pieces varied partially. Moreover, as a small change in the length of pieces also could be available and is effective in the final results, size determination in mm was carried out using a caliper, and these values for the width and length were used for further calculations (height, width, and length of bone-shaped samples are shown in Fig. 1B). A dog-bone-shaped sample was attached to the clamps of the probe (Cat.no. A/MTG, Stable Micro Systems LTD, Godalming, United Kingdom) of the texture analyzer while the starting point of the two clamps was 15.5 mm. During measurement, the sample was elongated by the upper clamp which moved up at a constant speed of 1 mm/s until the fracture point. From the values obtained from the texture analyzer, the fracture strain ($\mathcal{E}$, -) and true stress (σ, Pa) were calculated using Eqs. (2) and (3), respectively (Schreuders et al., 2019):

$$\varepsilon_h = \ln\frac{h(t)}{h_0} \quad (2)$$

$$\sigma(t) = \frac{F(t)}{A(t)} \quad (3)$$

$$A(t) = \frac{h_0}{h(t)} * A_0 \quad (4)$$

In these equations, h_0 is the initial height (m) of the sample (12 mm) and $h(t)$ is the height at time t. $F(t)$ is the force in Newton at time t, and $A(t)$ is the area at time t. To calculate the area (m^2) at time t, $A(t)$, Eq. (4) is used. In this equation, A_0 is the initial area (m^2) of dog-bone-shaped samples before the measurement and is calculated by multiplying the width and length of dog-bone-shaped samples. Young's modulus (kPa) was calculated from the initial, linear slope of the stress-strain curve. Finally, the anisotropic index (AI), which is a measure of the mechanical anisotropy in the products, is calculated by dividing the parallel data points by the perpendicular data points of either the stress or strain data using Eqs. (5) and (6), respectively:

$$AI_{stress} = \frac{\sigma_{parallel}}{\sigma_{perpendicular}} \quad (5)$$

$$AI_{strain} = \frac{\varepsilon_{parallel}}{\varepsilon_{perpendicular}} \quad (6)$$

Each formulation (Table 1) was made in triplicate and, thus, three sheared products were prepared. Then, for each replicate (sheared product), three perpendicular and three parallel cuts were tested, and the average value of three cuts was calculated for each replicate. Finally, the average of three values of three replicates and their standard deviations (SD) were calculated and reported in this study.

2.2.8. Statistical analysis

Complete Randomized Design (CRD) and SPSS statistical software (version 27.0, IBM, Armonk, NY, USA) were used to compare control (product without CYS or AA) and products containing the additives of CYS or AA (at concentrations of 100, 500, 1000, and 2000 ppm) described in Table 1. A descriptive Duncan's test was used to evaluate any statistical significance between samples at a significant level of 95% ($P \leq 0.05$). All reported data are shown as mean ± SD and all the tests were done in triplicate unless mentioned otherwise.

3. Results and discussion

3.1. Macrostructure visualization

3.1.1. Visualization of fiber formation

Fiber formation was visually assessed after folding the samples with the rupture parallel to the shear direction. Fig. 2 shows that the control sample (PPI-WG without CYS or AA) had a layered structure without recognizable fibers. Schreuders et al. (2019) reported a fibrous structure in PPI-WG product processed under the same conditions (PPI-WG, 120 °C, 39.1 s^{-1}, 15 min) but with 1% sodium chloride salt in its formulation, which might explain the difference. Salt was not used in this study to prevent any complications on the effects of the CYS or AA additives. Fig. 2 shows that clear and relatively large fibers were visible in the sample containing 2000 ppm of CYS in Fig. 2; however, a

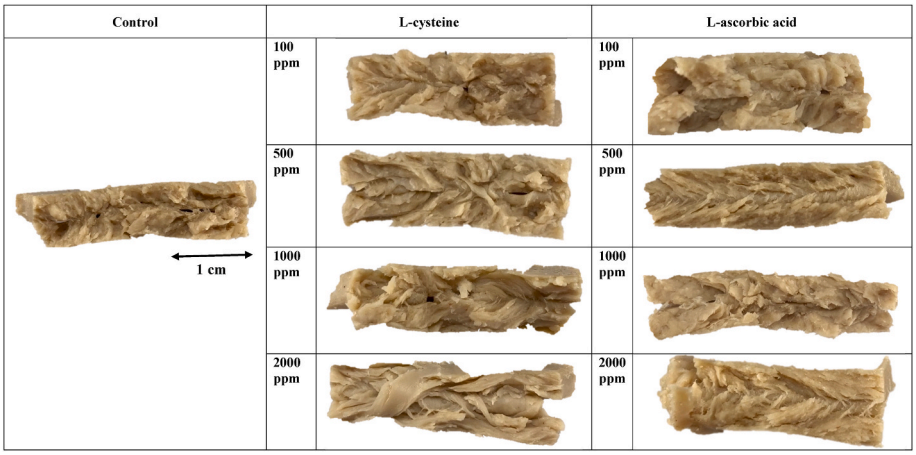

Fig. 2. Images of the fibrous structures of meat analogues formed after HTSC processing including the control and various concentration of L-cysteine and L-ascorbic acid (100, 500, 1000 and 2000 ppm). The meat analogues were folded parallel to the shearing direction.

concentration of 2000 ppm AA resulted only in smaller fibers. For both additives (CYS and AA), a lower concentration (100 ppm) resulted in a more layered structure, similar to the control. However, some fibrous structures became apparent as CYS and AA were added at 500 ppm with increasing intensity as the concentrations increased. Further analysis of the obtained structures will be presented in the following sections related to CLSM and SEM.

3.1.2. Browning index of products

The browning index (BI) shows the brown color purity and is an important parameter associated with browning where enzymatic and non-enzymatic browning occur (Bal, Kar, Satya, & Naik, 2011). BI increases by increasing a* and b* color parameters. Fig. 3 depicts the browning index of products containing CYS and AA at different concentrations (100, 500, 1000 and 2000 ppm) as well as the control (C) sample without any additives. The sample containing 2000 ppm of AA (AA-2000) exhibited the highest browning value (59.48 ± 2.26) with the sample containing 1000 ppm of CYS (CYS-1000) having the lowest value (43.85 ± 1.68). However, the browning index of CYS-1000 was not significantly lower than those of CYS-2000 (44.62 ± 1.51) and CYS-500 (45.82 ± 1.09) treatments ($P > 0.05$). The browning is reduced (−13.26%) when increasing the CYS concentration from 100 to 2000 ppm. In contrast, it is increased (+11.05%) with increasing concentration of AA from 100 ppm to 2000 ppm. The browning of the control (51.34 ± 0.40) is not significantly different from that of CYS-100, AA-100 and AA-500 ($P > 0.05$) but is significantly higher than the other samples treated with CYS and lower than the other samples treated with AA ($P \leq 0.001$).

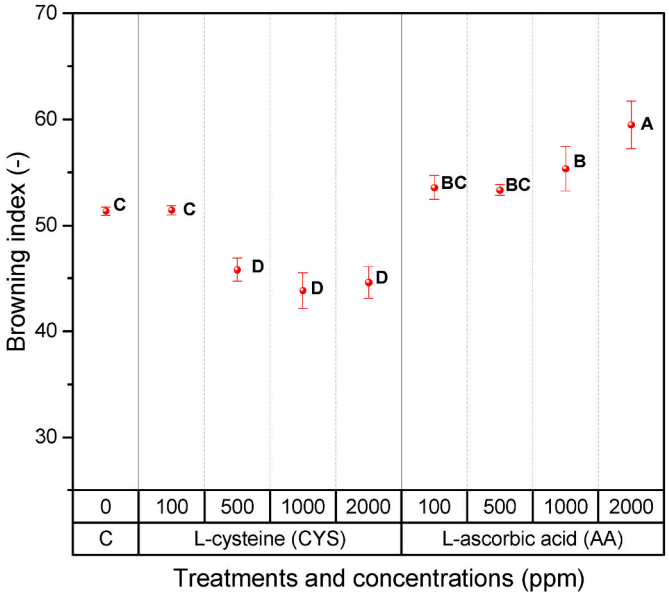

Fig. 3. Browning index (−) for the control (C), L-cysteine and L-ascorbic acid at different concentrations (100, 500, 1000 and 2000 ppm). Data are shown as the mean value ± SD. Mean values with different lower-case letters are significantly different ($P \leq 0.001$).

According to Li and Lee (1996), the whiteness value of the extrudates was increased and, thus, the browning index decreased as CYS (15000 ppm) was added to wheat flour extrudates. More recent studies suggest that the addition of CYS may lead to inhibition of the Maillard non-enzymatic browning reaction (S. Yang, Zhang, Li, Niu, & Yu, 2021; Zhang et al., 2018) due to its redox potential. In other words, CYS interacts with intermediate compounds from the Maillard reactions, and dissipate free radicals that are created during heating and shearing (M Li & Lee, 1996) thus inhibiting or slowing Maillard reaction (Zhang et al., 2018). Moreover, CYS also inhibits enzymatic browning caused by polyphenol oxidase (Ali, El-gizawy, El-bassiouny, & Saleh, 2015; Dudley & Hotchkiss, 1988; Rajesh, Nagesh, Vikram, & Anita, 2006; Richard-forget, Goupy, & Nicolas, 1992); however due to the processing at 120 °C, the interference of CYS with the Maillard intermediates is the most apparent reason for the lower browning as polyphenol oxidase will be inactivated by extensive heating at 120 °C for 15 min (Iqbal et al., 2018). However, due to the inherent presence of polyphenol oxidase in wheat, these mechanisms should not be excluded as a probable cause, for example during heating (Anderson & Morris, 2003).

Regarding the effect of ascorbic acid on increasing the browning index, Obradovic, Babic, Šubaric, Jozinovic, and Ackar (2015) reported that adding ascorbic acid to corn before extrusion preserves the carotenoids which influences the color of the extrudates. A recent paper suggested that even though a significant amount of AA is reduced (10–63%) during extrusion due to the high-temperatures (100/150/150 °C), carotenoids were protected in corn extrudates (Obradović et al., 2021). These papers are in good agreement with the results reported in this part of our study; and therefore, we expect that AA still adds color by preserving other colorants.

3.2. Microstructure

3.2.1. Confocal laser scanning microscopy (CLSM)

Fig. 4 depicts the images of sheared PPI-WG products captured by the CLSM to examine the spatial distribution of PPI and WG in the samples. In this figure, the control is shown on the left side whereas products with increasing concentrations of CYS and AA are shown in the middle and

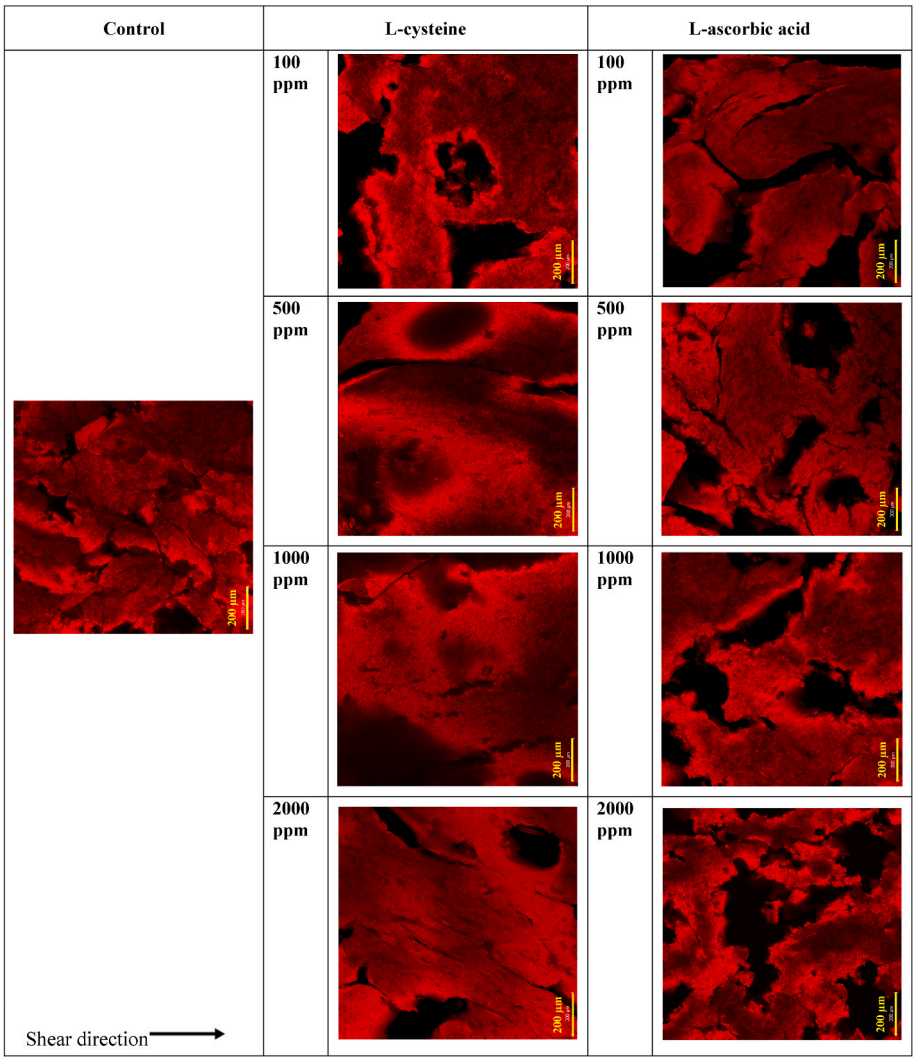

Fig. 4. CLSM images of 40 wt% PPI-WG (50/50 by weight) meat analogues without L-cysteine and L-ascorbic acid additives (Control) as well as meat analogues with different concentrations of L-cysteine and L-ascorbic acid (100, 500, 1000 and 2000 ppm) sheared by HTSC and stained with Rhodamine B.

left columns, respectively. According to Schreuders et al. (2019), WG attains a higher intensity of the red color than PPI in CLSM pictures of products containing WG and PPI due to the stronger affinity of Rhodamine B for WG and its higher local concentration due to its lower water binding relative to PPI. Dekkers, Emin, Boom, Jan, and Goot (2018) showed clearly that by increasing WG in WG-SPI products, the high intensity red color increased in CSLM pictures. They also concluded that the red intensity differences between SPI and WG resulted from differences in the Rhodamine B affinity to the proteins and the difference in protein concentrations in each phase. These researchers showed that WG absorbed less water and, thus, resulted in a more concentration of WG in that phase and higher intensity in the red color. Moreover, Schreuders et al. (2020) showed similar water distribution of SPI and PPI and always larger than that for WG at similar dry matter content using time-domain NMR relaxometry (TD-NMR). Fig. 4 shows different color intensities, but the alignment in the shear direction in the control sample is not as evident as that in the paper of Schreuders et al. (2019) which uses the same conditions (PPI + WG, 120 °C, 39.1 s^{-1}, 15 min) albeit with 1% sodium chloride salt added to the formulation.

Figs. 4 and 5 show that as the concentration of CYS increases from 100 ppm to 2000 ppm, the pores and thus the black color reduces significantly ($P \leq 0.05$), and a more compact structure is obtained at CYS-2000. Moreover, CYS-2000 has a significantly more ($P \leq 0.05$) low-intensity red color than other samples containing CYS. Therefore, although the amount of high-intensity red color is not significantly different between samples containing CYS ($p > 0.05$), the ratio of high-intensity red color to low-intensity red color decreases from CYS-100 to CYS-2000 and high-intensity red regions are somewhat reduced in the CYS-2000. A possible explanation could be that CYS reduced the number of crosslinks in the WG. As a consequence, WG can absorb more water, which could lead to smaller differences in water contents between WG and PPI (Cornet, van der Goot, & van der Sman, 2020). Moreover, one may expect that as CYS facilitates breakup of internal S–S bridges, it will accelerate the formation of new bridges between PPI and WG during HTSC processing (Fig. 6), which will accelerate mixing in the material and reduce the inhomogeneity in composition. Li and Lee (1996) suggested that proteins can form a homogeneous suspension when mixed with water at high temperatures. Thus, protein chains are denatured and dissociated, which could facilitate the alignment of the protein phase in the direction of the shear flow. These denatured and mixed proteins then aggregate by hydrophobic interaction and S–S cross-linking (M Li & Lee, 1996) represented in Fig. 6.

Upon CYS addition, denser packing with less pores occurred as the CYS concentration was increased to 2000 ppm (Figs. 4 and 5). In fact, the addition of CYS could lead to the formation of larger fibers and a layered structure (Fig. 2), though the presence of fibers was not reflected in anisotropy in the mechanical tests. The apparent effect that CYS exhibited at elevated concentrations happened in both parallel and

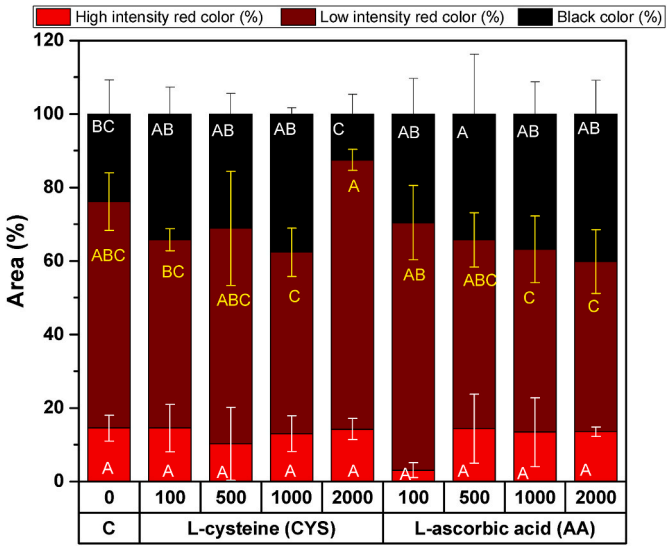

Fig. 5. The areas of black color and high and low intensity red colors in the CSLM pictures. For low intensity red color and black color, different letters inside each bar indicate a significant difference of $P \leq 0.05$. For high intensity red color, there is not a significant difference between treatments ($P > 0.05$). (For interpretation of the references to color in this figure legend, the reader is referred to the Web version of this article.)

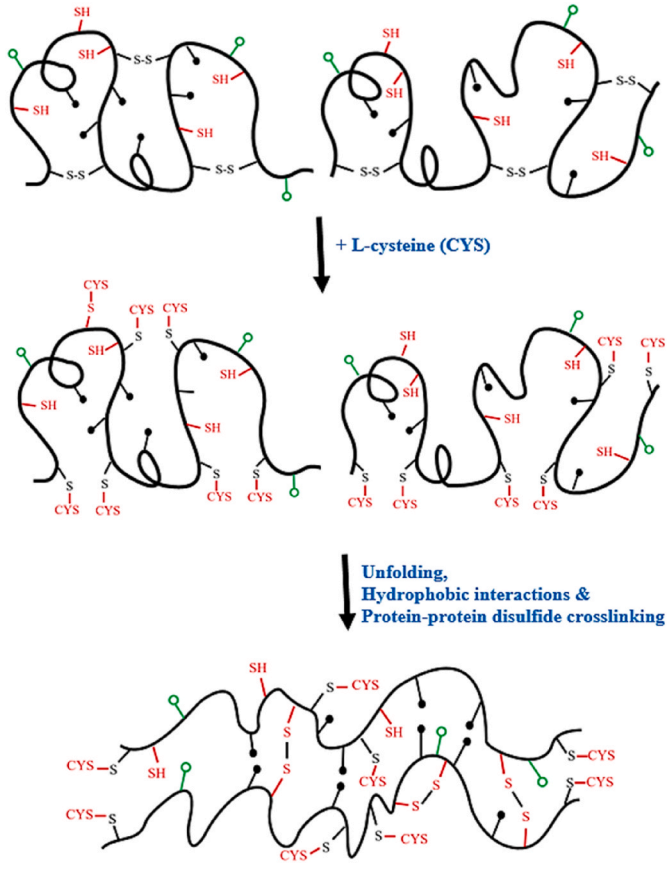

Fig. 6. Schematic diagram of the proposed effect of L-cysteine (CYS) addition on proteins and following denaturation and alignment of proteins in the direction of shear flow in the HTSC and cross-linking of proteins chains through hydrophobic interactions and disulphide (S–S) bonds. In this figure, black solid circles and hollow green circles show the hydrophobic and hydrophilic amino acid side chains, respectively. (For interpretation of the references to color in this figure legend, the reader is referred to the Web version of this article.)

perpendicular directions simultaneously as can be concluded from Fig. 4. The denser packing could be caused by breaking of S–S bridges due to CYS's reducing effects, which decrease steric hindrance and, thus, enable the protein chains to come into closer proximity. As reactive sites come into closer proximity, redistribution of the covalent S–S bonds between proteins could result in a denser matrix (Fig. 6). It is suggested that the CYS can result in protein polymerization through SH- SS interchange reactions during the heat processing to create a continuous covalent network in the proteins upon cooling. Therefore, the addition of CYS could be advantageous due to the S–S rearrangement (Were, Hettiarachchy, & Coleman, 1999). In fact, during HTSC processing similar to the extrusion processing due to shear force, heat and pressure, protein cross-linking by noncovalent (especially hydrophobic bonds) and covalent bonds (especially S–S bonds) can result in an increase in molecular weight, protein polymerization, and formation of a protein network (Mei Li & Lee, 1998). Thus, the application of CYS in the sample could break the S–S bonds of proteins in the first step and, then, densify the protein phase following the mechanism described above (Fig. 6). The effect could enable the alignment of protein phases in the direction of the shear flow (Fig. 4). Therefore, at the same time, the orientation of domains to the shear can be observed, in combination with a compact packing at 2000 ppm.

The addition of AA caused different effects as can be clearly seen in Fig. 4. The materials containing AA at elevated concentrations (500, 1000 and 2000 ppm) show large pores (black areas) in Fig. 4 within the microstructure, which are not completely aligned to the shear direction. Fig. 2 suggested the presence of (small) fiber in products containing AA concentrations of 500 and 2000 ppm from a macrostructure perspective. The CLSM images depicted in Fig. 4 show these fibers and elongated pores at a microscopic scale for AA-2000 ppm. Moreover, Figs. 4 and 5 show that as the concentrations of AA increased, the high-intensity red regions were somewhat increased, and the low-intensity red color decreased. Fig. 5 shows that by increasing the concentration of AA from 100 to 2000 ppm, the black color (pores and openings) increased significantly ($P \leq 0.05$). This can confirm the oxidizing effect of AA especially, on WG. In this case, it increased the crosslink density in WG and reduced the water absorption by WG. Therefore, the difference between WG and PPI increased more, and, thus, the bright red color of WG increased by increasing AA concentration.

3.2.2. Scanning electron microscopy (SEM)

The results of the SEM at magnification 250X are depicted in Fig. 7. The shear flow direction is also shown in this figure. Alignment to the shear flow direction is observed with most materials except with CYS-100. Fig. 7 confirms the dense, layered matrix obtained with 2000 ppm of CYS found in Fig. 4. These layers could be part of the large fibers that were observed visually in Fig. 2. As the CYS reduces the intramolecular crosslinks and breaks the protein chains, it will allow higher protein mobility, more deformation of the molecules under shear, and thus, more re-organization of the crosslinks. Then, intermolecular crosslinking takes place (Peng et al., 2022), which results in a denser matrix. Peng et al. (2022) also reported a dense matrix with PPI after the addition of 900 ppm CYS using extrusion. They concluded that the re-organization of the crosslinks due to CYS addition resulted in an improved fibrous structure in the cooling die of the extruder. It could also be attributed to the bonding of CYS to the protein, changing protein chemical composition, promoting protein interactions and reducing protein molecular weight. Figs. 7 and 5 also showed that as the concentration of AA increases, the number of porosities within the structure increases. This would be in accordance with the described mechanism, where DHAA quickly re-crosslinks the molecules, creating stronger patches that will behave as solid particles, which cannot deform much and therefore will be surrounded by pores. In general, SEM confirmed our findings with CLSM and visual inspection. For instance, AA-2000 clearly depicts small fibers in Fig. 7, which directly correspond to the fibers that were found in Fig. 2. Some degree of anisotropy can also be

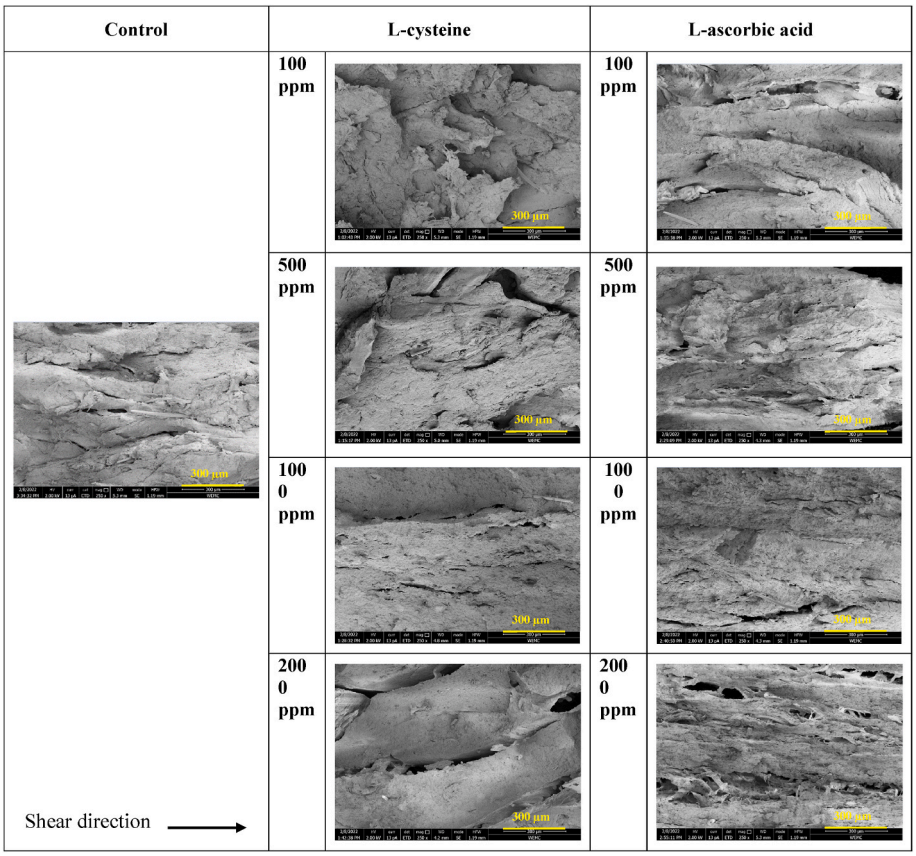

Fig. 7. SEM images at magnification 250X for the control and meat analogues with various concentrations (100, 500, 1000 and 2000 ppm) of L-cysteine and L-ascorbic acid.

observed as the alignment of the formed pores is strictly parallel to the shear direction for the AA-2000 sample in Fig. 7.

3.3. Mechanical properties

3.3.1. Tensile stress, tensile strain and Young's modulus

The values for the tensile stress, tensile strain and Young's modulus for both parallel and perpendicular directions of all products are shown in Fig. 8 A, B, and C, respectively. Fig. 8 A and B show that the highest values for the parallel and perpendicular directions of tensile stress (89.71 ± 6.91 kPa and 86.98 ± 8.43 kPa, respectively) and tensile strain (0.40 ± 0.06 and 0.40 ± 0.02, respectively) were obtained for CYS-2000. Those values were significantly different from all other data points ($P \leq 0.001$). Moreover, the tensile stress and strain of products in both parallel and perpendicular directions increased when the CYS concentration increased from 0 to 2000 ppm. Although a similar trend can be seen with AA, it is less clear for the perpendicular direction of samples containing AA. We expect that this is related to the high porosity of the materials created with AA.

Fig. 8 C illustrates a significant increase of Young's modulus ($P \leq 0.001$) within parallel extracted samples as compared to the control (130.20 ± 3.41 kPa) was obtained for both additives from a concentration of 500+ ppm except for AA-2000 (150.15 ± 2.91 kPa). Moreover, this figure shows that perpendicular extracted samples again depict the elevated Young's modulus as the concentration of CYS was increased. In fact, CYS-2000 (197.39 ± 27.84 kPa) and CYS-1000 (197.12 ± 8.74 kPa) exhibited the highest Young's modulus values in perpendicular direction while being insignificantly different ($p > 0.05$) with CYS-500 (181.44 ± 19.87 kPa) and AA-500 ppm (177.21 ± 17.79 kPa). In fact, as the increase of tensile stress for samples containing CYS, especially at higher concentrations of 1000 and 2000 ppm is much higher (Fig. 8 A) than the increase of their tensile strain data (Fig. 8 B), Young's modulus increases by increasing CYS concentration from 0 to 2000 ppm (Fig. 8 C).

Higher stress, strain and Young's Modulus in products containing PPI and WG proteins suggest the creation of additional polymer cross-links. More crosslinks are reported to lead to an increased sample strength, enhanced restoring capacity after deformation, and higher resistance to extension (Abang Zaidel, Chin, Abdul Rahman, & Karim, 2008). Important is here the formation of intermolecular crosslinks created during processing, accelerated and enhanced by the presence of the reductor. Intermolecular crosslinks do not necessarily contribute to the macroscopic strength of a material, since it will break in between the molecules, which are not covalently connected. Intermolecular cross-links, however, will increase the strength as soon as the overall crosslink density exceeds a certain percolation threshold.

Regarding the application of CYS and after breaking S–S bonds in the first step by CYS, S–S bonds play a key role in protein crosslinking as two SH groups could be linked within one protein (intrachain), or between two proteins (interchain) in the next step (Lutz, Wieser, & Koehler, 2012). Strecker, Cavalieri, Zollars, and Pomeranz (1995) reported that a small increase in S–S bond leads to a great intensification in network formation in wheat proteins. This confirms that S–S bonds are effective on to the polymerization of proteins (Strecker et al., 1995). Moreover, it was found that the protein S–S content had a significant positive correlation to wheat dough hardness (Manu & Prasada Rao, 2008). Koh, Karwe, and Schaich (1996) also reported that S–S increased in wheat flour extrudates with added CYS. In fact, the rise in S–S bonds could be because of the bonding between protein and CYS, two CYS molecules, or two proteins. The reduction of SH groups could be because of development of SS bonds. Moreover, CYS degradation and creation of other compounds containing sulfur during the processing could be other

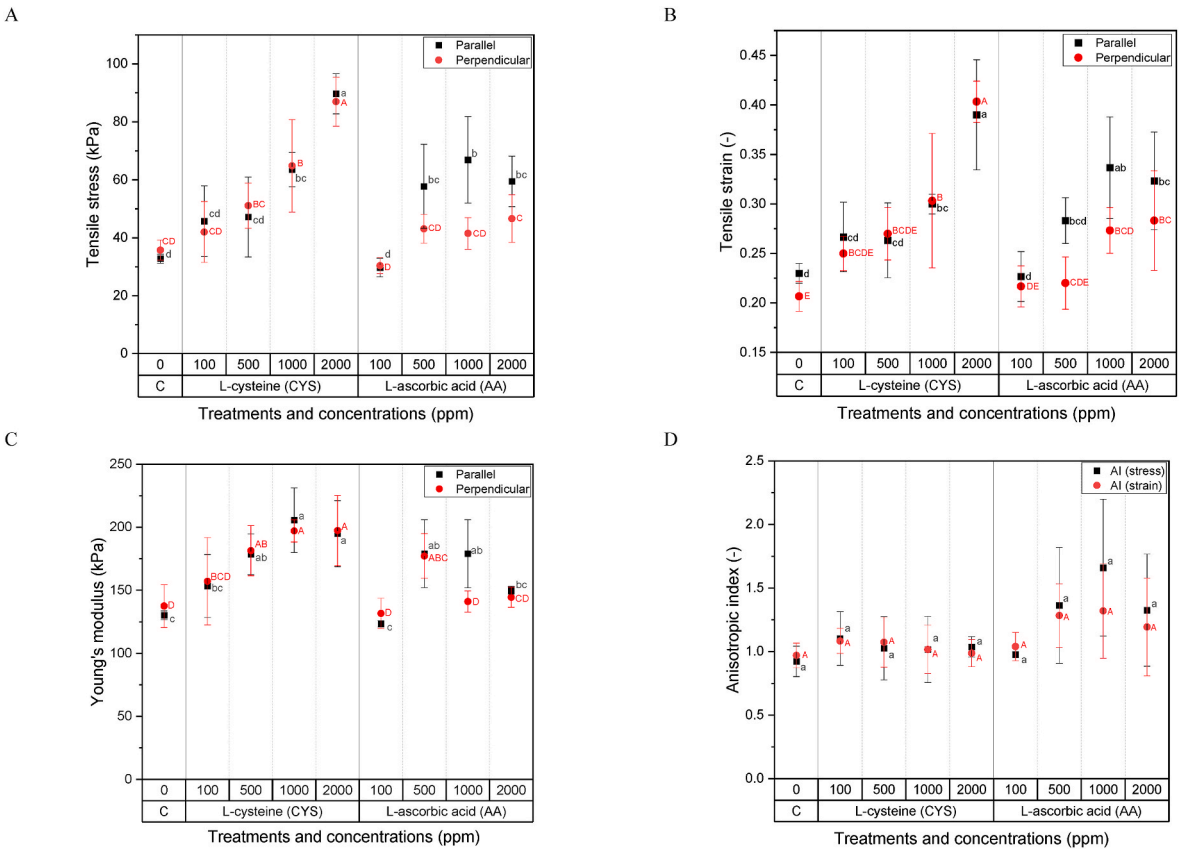

Fig. 8. Results for the A) tensile stress, B) tensile strain, C) Young's modulus and D) anisotropic index of meat analogues in parallel (■) and perpendicular (●) directions. Lower case letters correspond with parallel data points whereas, upper case letters correspond with perpendicular data points. There is not a significant difference for AI parameter ($P > 0.05$). For other parameters, different letters next to the data points indicate a significant difference of ($P \leq 0.001$).

reasons for the reduction of SH groups (M Li & Lee, 1996). Regarding the increasing strength of samples, it seems that the rise in S–S bonds is mostly due to the bonding of SH groups between proteins and production of S–S bonds. Peng et al. (2022) reported that the hardness of pea protein extrudate increased by increasing the concentration of CYS from 0 to 900 ppm due to the cross-linking changing of the S–S bonds between pea protein molecules. These researchers reported the reduction of free SH groups probably by their oxidation into a S–S bond upon addition of CYS (Peng et al., 2022). Similar to our results, Were et al. (1999) reported that the tensile strength of films produced by soy-wheat proteins was enhanced with CYS addition at pH 7.0 because of an increase in S–S bond formation by CYS. Therefore, the data in Fig. 8 A, B and C could suggest an increase in cross-linking of products by increasing the concentration of CYS which could indicate the effect of CYS on S–S bond formation, especially on wheat gluten. WG contains a considerable amount of L-cysteine (Chiang et al., 2021) and a relatively more than PPI (Cornet, Snel, et al., 2020). Therefore, the effect of CYS on WG could be more.

When CYS works as a reducing agent, it is beneficial to break the secondary structure of protein molecules, and then, it promotes the crosslinking of the intermolecular S–S bonds and polymerization of protein to improve its rheological and textural properties. Concurrent shear then can break the weaker intramolecular hydrophobic and hydrogen interactions and deform the molecules strongly enough to allow for the creation of intermolecular crosslinks. In more detail, as Fig. 6 shows the unfolded proteins can then be incorporated into the protein network, first by hydrophobic and hydrogen interaction and then S–S crosslinking (N. Yang, Qian, Jiang, & Hou, 2021) and, thus, a more compact and dense protein structure could be created. Therefore, the densely packed matrix that is observed at elevated concentrations of CYS (in Figs. 4, 6 and 7) correlates with larger tensile strain and stress (Fig. 8 A and B, respectively) and an increased Young's modulus (Fig. 7 C).

The increased stress and strain of materials created with AA in Fig. 8 A and B can be explained by the same mechanism. Although a decrease in the mean values of the stress and strain (in Fig. 8 A and B, respectively) can be observed in the parallel direction by increasing the concentration of AA from 1000 to 2000 ppm, these reductions are not significant. These reductions may be due to the depletion of oxygen in the closed beaker during the hydration process at high AA concentrations (such as 2000 ppm) in the protein mixture. In this case, AA cannot be oxidized to DHAA which is the real oxidizing agent (Stoica et al., 2013). In wheat, the endogenous protein disulfide isomerase (PDI), catalyzes SH/SS exchange reactions and AA is involved in this mechanism (D. Every, Simmons, & Ross, 2006; Joye et al., 2009). Thus, this mechanism results in more S–S bonds and a stronger network which could increase the tensile stress and strain. Regarding the effect of AA, it was reported that it could positively affect the sample hardness and quality by improving the stability of gluten network (Sheikholeslami, Karimi, Reza, & Mahfouzi, 2018). Ndayishimiye et al. (2016) reported that treatment of sweet potato–wheat dough with AA increased the molecular weight of polymers (Ndayishimiye et al., 2016). In fact, AA could oxidize to DHAA in the presence of oxygen and then, it oxidizes reduced glutathione into an oxidized form in the wheat dough. Then, the exchange of S–S bonds between polypeptide chains could stabilize and immobilize the protein by facilitating hydrophobic interactions and hydrogen bonding in the protein (Ndayishimiye et al., 2016). We believe that DHAA is very quick in the oxidation of SH groups, as many of the new bridges are still intramolecular. Therefore, the strengthening effect is much less than CYS. At the same time, the formation of more

intramolecular (local) crosslinks by DHAA results in rather solid patches, which then cannot yield on the overall structure, and, thus, leads to the formation of pores, which act as nuclei for rupture under deformation. This leads to unclear trends, but also to the difference between parallel and perpendicular directions.

3.3.2. Anisotropic index (AI)

The data presented in Fig. 8 D represent the AI of different products described in Table 1. This figure shows that all products containing different concentrations of CYS (0–2000 ppm) as well as AA-100 are all near the isotropy (strain and stress) of 1.0. It is because of the relatively small differences between parallel and perpendicular data points of tensile stress and strain as can be observed in Fig. 8 A and B, respectively. In Fig. 8 D, the highest mean value of the AI (strain) was observed for AA-1000 (1.32 ± 0.37) whereas, the lowest mean value was observed for the control (0.97 ± 0.10). However, none of the data points of the AI (strain) differ significantly ($p > 0.05$). Comparable to the AI data based on tensile strain, the highest mean value for the AI (stress) parameter was observed for AA-1000 (1.66 ± 0.54). However, none of the data points of the AI (stress) differ significantly ($p > 0.05$).

Therefore, although somewhat insignificant, the products containing elevated amounts (500–2000 ppm) of AA hint at increased anisotropy. This corresponds with the small observable fibers in AA-2000 and AA-1000 in Fig. 2. The fibers observed for CYS-2000, however, do not lead to mechanical anisotropy as can be seen in Fig. 8 D. One possible interpretation of the observed fibers in CYS-2000 could be that the effect of CYS on the sample is isotropic and happens in all directions, simultaneously. This resulted in a layered structure and formation of big fibers as the concentration of CYS was increased, especially at 2000 ppm. It increases both the tensile strain and stress (Fig. 8 A and B, respectively) in both parallel and perpendicular directions. Therefore, the differences between the tensile strain and stress in parallel and perpendicular directions remain stable for samples containing CYS. This becomes evident as the AI (Fig. 8 D) of both tensile stress and strain became close to 1 for these samples. In other words, it is hypothesized that AI does not increase considerably when big fibers and a layered structure are formed. However, this layered structure could increase Young's modulus (Fig. 8 C).

Moreover, the air holes and pores enforce local alignment of the fibers and could further increase the anisotropy of the material. According to the paper of Wang, Tian, Boom, and van der Goot (2019), the mechanical anisotropy of a calcium caseinate (30 w/w %), which was shear-induced, is caused by a combination of anisotropy in the protein phase and the entrapped air phase (Wang et al., 2019). In fact, the visual appearance of products using CSLM and SEM (Figs. 4 and 7, respectively) in our study also showed fractures or voids were formed in products with higher CYS and AA concentrations. On the other hand, porosity, which can be visualized by CLSM and SEM, could present valuable data on the degree to which air is entrapped in the matrix (Schreuders et al., 2019). Some degree of anisotropy can be observed as the alignment of the formed pores is strictly parallel to the shear direction for the AA-2000 sample in Fig. 6. This observation can directly be correlated to the elevated AI (>1) as AA concentration increased in Fig. 8 D. However, a densely packed matrix of samples containing CYS resulted in AI values relatively close to 1 even though the concentration of CYS was increased (Fig. 8 D).

4. Conclusion

In this study, a mixture of WG and PPI was used to produce anisotropic products using HTSC technology. This exploratory research was aimed at investigating the possible application of L-ascorbic acid (AA) and L-cysteine (CYS) at different concentrations (100, 500, 1000 and 2000 ppm) in the formulation of the protein blends to improve their fibrous and textural properties. The results showed that CYS had big effects on color and strength and less on fibrousness and anisotropy of the products. Visualization of the microstructure of L-cysteine-containing samples using CLSM and SEM illustrated a densely packed layered structure with fewer pores, especially at a high concentration of 2000 ppm. CYS led to reorganization and probably more swelling of WG. That makes differences between WG and PPI smaller, giving low opportunities to make anisotropic structures. When WG absorbs more water, then PPI will have less water. That could make the blend stronger overall. AA increased the browning index of products and had a smaller effect on mechanical properties, but it increased the production of small fibers. These results can be correlated with microstructural results obtained by CLSM and SEM as AA led to more crosslinks and stronger WG, which can be an explanation for its effect on fiber formation. In summary, the results of this study confirmed a potential benefit of CYS and/or AA on the textural properties of products containing WG and PPI and sheared by HTSC. The application of 2000 ppm CYS or AA can improve the textural and sensorial properties of meat analogues. However, future in-depth research surrounding the effect of HTSC process parameters especially, the temperature on the application of these additives could reveal possible applications within the meat analogue industry. Moreover, sensorial analysis of meat analogues containing these additives by the consumers is suggested for future research. Finally, as gluten-free products are demanded by celiac patients, the production of meat analogues without gluten and containing these additives should be investigated in the next research.

Author statement

Somayeh Taghian Dinani: Term, Conceptualization, Formal analysis, Validation, Visualization, Writing - Review & Editing; **Jeroen Philip van der Harst**: Investigation, Formal analysis, Validation, Visualization, Writing - Original Draft; **Remko Boom**: Supervision, Funding acquisition, Writing - Review & Editing; **Atze Jan van der Goot**: Term, Conceptualization, Supervision, Funding acquisition, Writing - Review & Editing.

Declaration of competing interest

All authors declare that there is no conflict of interest.

Data availability

Data will be made available on request.

Acknowledgment

The authors would like to thank Jarno Gieteling, Jos Sewalt, Maurice Strubel, Wouter de Groot, Martin de Wit and Jelmer Vroom for their great technical support.

References

Abang Zaidel, D. N., Chin, N. L., Abdul Rahman, R., & Karim, R. (2008). Rheological characterisation of gluten from extensibility measurement. *Journal of Food Engineering, 86*(4), 549–556. https://doi.org/10.1016/j.jfoodeng.2007.11.005

Ali, H. M., El-gizawy, A. M., El-bassiouny, R. E. I., & Saleh, M. A. (2015). Browning inhibition mechanisms by cysteine , ascorbic acid and citric acid , and identifying PPO-catechol-cysteine reaction products. https://doi.org/10.1007/s13197-014-1437-0, 52(June), 3651-3659.

Anderson, J. V., & Morris, C. F. (2003). Purification and analysis of wheat grain polyphenol oxidase (PPO) protein. *Cereal Chemistry, 80*(2), 135–143. https://doi.org/10.1094/CCHEM.2003.80.2.135

Bal, L. M., Kar, A., Satya, S., & Naik, S. N. (2011). Kinetics of colour change of bamboo shoot slices during microwave drying. *International Journal of Food Science and Technology, 46*(4), 827–833. https://doi.org/10.1111/j.1365-2621.2011.02553.x

Banerjee, S., & Bhattacharya, S. (2012). Food gels: Gelling process and new applications. *Critical Reviews in Food Science and Nutrition, 52*(4), 334–346. https://doi.org/10.1080/10408398.2010.500234

Bildstein, M., Lohmann, M., Hennigs, C., Krause, A., & Hilz, H. (2008). An enzyme-based extraction process for the purification and enrichment of vegetable proteins to be

applied in bakery products. *European Food Research and Technology, 228*(2), 177–186. https://doi.org/10.1007/s00217-008-0921-z

Boye, J., Zare, F., & Pletch, A. (2010). Pulse proteins : Processing , characterization , functional properties and applications in food and feed. *Food Research International, 43*(2), 414–431. https://doi.org/10.1016/j.foodres.2009.09.003

Cederberg, C., & Flysjö, A. (2004). *Environmental assessment of future pig farming systems – quantifications of three scenarios from the FOOD 21 synthesis work*.

Chiang, J. H., Tay, W., Ong, D. S. M., Liebl, D., Ng, C. P., & Henry, C. J. (2021). Physicochemical, textural and structural characteristics of wheat gluten-soy protein composited meat analogues prepared with the mechanical elongation method. *Food Structure, 28*. https://doi.org/10.1016/j.foostr.2021.100183. September 2020.

Cornet, S. H. V., Snel, S. J. E., Schreuders, F. K. G., van der Sman, R. G. M., Beyrer, M., & van der Goot, A. J. (2020). Thermo-mechanical processing of plant proteins using shear cell and high-moisture extrusion cooking. *Critical Reviews in Food Science and Nutrition*, 1–18. https://doi.org/10.1080/10408398.2020.1864618, 0(0).

Cornet, S. H. V., van der Goot, A. J., & van der Sman, R. G. M. (2020). Effect of mechanical interaction on the hydration of mixed soy protein and gluten gels. *Current Research in Food Science, 3*, 134–145. https://doi.org/10.1016/j.crfs.2020.03.007

Davis, J., Sonesson, U., Baumgartner, D. U., & Nemecek, T. (2010). Environmental impact of four meals with different protein sources : Case studies in Spain and Sweden. *Food Research International, 43*(7), 1874–1884. https://doi.org/10.1016/j.foodres.2009.08.017

Day, L., & Swanson, B. G. (2013). Functionality of protein-fortified extrudates. *Comprehensive Reviews in Food Science and Food Safety, 12*(5), 546–564. https://doi.org/10.1111/1541-4337.12023

Dekkers, B. L., Emin, M. A., Boom, R. M., Jan, A., & Goot, V. Der (2018). The phase properties of soy protein and wheat gluten in a blend for fi brous structure formation. *Food Hydrocolloids, 79*, 273–281. https://doi.org/10.1016/j.foodhyd.2017.12.033

Dudley, E. D., & Hotchkiss, J. H. (1988). Cysteine as an inhibitor of polyphenol oxidase. *Journal of Food Biochemistry, 13*(1989), 65–75.

Every, D., Motoi, L., Rao, S. P., Shorter, S. C., & Simmons, L. D. (2008). Inhibition mechanism of L-cysteine on maillard reaction by trapping 5-Hydroxymethylfurfural. *Journal of Cereal Science, 48*(48), Article 339e348. https://doi.org/10.1016/j.jcs.2007.10.002

Every, D., Simmons, L. D., & Ross, M. P. (2006). Distribution of redox enzymes in millstreams and relationships to chemical and baking properties of flour. *Cereal Chemistry, 83*(1), 62–68. https://doi.org/10.1094/CC-83-0062

Gizzarelli, F., Corinti, S., Barletta, B., Iacovacci, P., Brunetto, B., Butteroni, C., et al. (2006). Evaluation of allergenicity of genetically modified soybean protein extract in a murine model of oral allergen-specific sensitization. *Clinical and Experimental Allergy, 36*(2), 238–248. https://doi.org/10.1111/j.1365-2222.2005.02415.x

Grabowska, K. J., Zhu, S., Dekkers, B. L., De Ruijter, N. C. A., Gieteling, J., & Van Der Goot, A. J. (2016). Shear-induced structuring as a tool to make anisotropic materials using soy protein concentrate. *Journal of Food Engineering, 188*, 77–86. https://doi.org/10.1016/j.jfoodeng.2016.05.010

Grabowska, K. J., Zhu, S., Dekkers, B. L., Ruijter, N. C. A. De, Gieteling, J., & Goot, A. J. Van Der (2016). Shear-induced structuring as a tool to make anisotropic materials using soy protein concentrate. *Journal of Food Engineering, 188*, 77–86. https://doi.org/10.1016/j.jfoodeng.2016.05.010

Hoek, A. C., Luning, P. A., Weijzen, P., Engels, W., Kok, F. J., & de Graaf, C. (2011). Replacement of meat by meat substitutes. A survey on person- and product-related factors in consumer acceptance. *Appetite, 56*(3), 662–673. https://doi.org/10.1016/J.APPET.2011.02.001

Hruskova, M., Novotna, D., Hrušková, M., & Novotná, D. (2003). Effect of ascorbic acid on the rheological properties of wheat fermented dough. *Czech Journal of Food Sciences, 21*, 137–144. https://doi.org/10.17221/3490-CJFS

Iqbal, A., Murtaza, A., Muhammad, Z., Elkhedir, A. E., Tao, M., & Xu, X. (2018). Inactivation, aggregation and conformational changes of polyphenol oxidase from quince (Cydonia oblonga Miller) juice subjected to thermal and high-pressure carbon dioxide treatment. *Molecules, 23*(7). https://doi.org/10.3390/molecules23071743

Joye, I. J., Lagrain, B., & Delcour, J. A. (2009). Endogenous redox agents and enzymes that affect protein network formation during breadmaking – a review. *Journal of Cereal Science, 50*(1), 1–10. https://doi.org/10.1016/j.jcs.2009.04.002

Kendler, C., Duchardt, A., Karbstein, H. P., & Emin, M. A. (2021). *Effect of oil content and oil addition point on the extrusion processing of wheat gluten-based meat analogues*.

Koh, B. K., Karwe, M. V., & Schaich, K. M. (1996). Effects of cysteine on free radical production and protein modification in extruded wheat flour. *Cereal Chemistry, 73*, 115–122.

Lambert, I. A., & Kokini, J. L. (2001). Effect of L-cysteine on the rheological properties of wheat flour. *Cereal Chemistry, 78*(3), 226–230. https://doi.org/10.1094/CCHEM.2001.78.3.226

Li, M., & Lee, T. (1996). Effect of cysteine on the functional properties and microstructures of wheat flour extrudates. *Journal of Agricultural and Food Chemistry, 44*(7), 1871–1880. https://doi.org/10.1021/JF9505741

Li, M., & Lee, T. C. (1998). Effect of cysteine on the molecular weight distribution and the disulfide cross-link of wheat flour proteins in extrudates. *Journal of Agricultural and Food Chemistry, 46*(3), 846–853. https://doi.org/10.1021/jf960825l

Lu, X., & Seib, P. A. (1998). Assay of dehydroascorbic acid in bread and dough added as a crystalline dimer. *Cereal Chemistry, 75*(2), 200–206. https://doi.org/10.1094/CCHEM.1998.75.2.200

Lutz, E., Wieser, H., & Koehler, P. (2012). Identification of disulfide bonds in wheat gluten proteins by means of mass spectrometry/electron transfer dissociation. *Journal of Agricultural and Food Chemistry, 60*(14), 3708–3716. https://doi.org/10.1021/jf204973u

Majzoobi, M., Farahnaky, A., Jamalian, J., & Radi, M. (2011). Effects of L-Cysteine on some characteristics of wheat starch. *Food Chemistry, 124*(3), 795–800. https://doi.org/10.1016/j.foodchem.2010.06.098

Manski, J. M., van der Goot, A. J., & Boom, R. M. (2007). Advances in structure formation of anisotropic protein-rich foods through novel processing concepts. *Trends in Food Science & Technology, 18*(11), 546–557. https://doi.org/10.1016/j.tifs.2007.05.002

Manu, B. T., & Prasada Rao, U. J. S. (2008). Influence of size distribution of proteins, thiol and disulfide content in whole wheat flour on rheological and chapati texture of Indian wheat varieties. *Food Chemistry, 110*(1), 88–95. https://doi.org/10.1016/j.foodchem.2008.01.060

Merkel, T., Emin, M. A., Schuch, A., & Schuchmann, H. P. (2015). Design of a cone-cone shear cell to study emulsification characteristics. *Chemical Engineering & Technology*, (2), 304–310. https://doi.org/10.1002/ceat.201400486

Michel, F., Hartmann, C., & Siegrist, M. (2021). Consumers' associations, perceptions and acceptance of meat and plant-based meat alternatives. *Food Quality and Preference, 87*(April 2020), Article 104063. https://doi.org/10.1016/j.foodqual.2020.104063

Ndayishimiye, J. B., Huang, W. N., Wang, F., Chen, Y. Z., Letsididi, R., Rayas-Duarte, P., et al. (2016). Rheological and functional properties of composite sweet potato – wheat dough as affected by transglutaminase and ascorbic acid. *Journal of Food Science & Technology, 53*(2), 1178–1188. https://doi.org/10.1007/s13197-015-2004-z

Obradović, V., Babić, J., Dragović-Uzelac, V., Jozinović, A., Ačkar, Đ., & Šubarić, D. (2021). Properties of extruded snacks prepared from corn and carrot powder with ascorbic acid addition. *Processes, 9*(8), 1367. https://doi.org/10.3390/PR9081367

Obradovic, V., Babic, J., Šubaric, D., Jozinovic, A., & Ackar, D. (2015). Physico-chemical properties of corn extrudates enriched with tomato powder and ascorbic acid. *Chemical and Biochemical Engineering Quarterly, 29*(3), 325–342. https://doi.org/10.15255/CABEQ.2014.2159

O'kane, F. E., Happe, R. P., Vereijken, J. M., Gruppen, H., & Boekel, J. S. V. A. N. (2004). Heat-induced gelation of pea legumin : Comparison with soybean glycinin. *Journal of Agricultural and Food Chemistry, 52*, 5071–5078.

Peng, H., Zhang, J., Wang, S., Qi, M., Yue, M., Zhang, S., et al. (2022). High moisture extrusion of pea protein: Effect of L-cysteine on product properties and the process forming a fibrous structure. *Food Hydrocolloids, 129*(266), Article 107633. https://doi.org/10.1016/j.foodhyd.2022.107633

Rajesh, G., Nagesh, D., Vikram, G., & Anita, A. (2006). Reversible inhibition of Polyphenol oxidase from apple using L-cysteine. *Indian Journal of Chemical Technology, 6*, 459–463.

Richard-forget, F. C., Goupy, P. M., & Nicolas, J. J. (1992). Cysteine inhibitor of enzymatic browning. 2. Kinetic studies. *Journal of Agricultural and Food Chemistry, 40*, 2108–2113.

Riha, W. E., Hwang, C.-F., Karwe, M. V., Hartman, T. G., & Ho, C.-T. (1996). Effect of cysteine addition on the volatiles of extruded wheat flour. *Journal of Agricultural and Food Chemistry, 44*(7), 1847–1850.

Schreuders, F. K., Bodn, I., Erni, P., Boom, R. M., Goot, A. J. Van Der, Bodnár, I., et al. (2020). Water redistribution determined by time domain NMR explains rheological properties of dense fibrous protein blends at high temperature. *Food Hydrocolloids, 101*. https://doi.org/10.1016/j.foodhyd.2019.105562

Schreuders, F. K. G., Dekkers, B. L., Bodnár, I., Erni, P., Boom, R. M., & van der Goot, A. J. (2019). Comparing structuring potential of pea and soy protein with gluten for meat analogue preparation. *Journal of Food Engineering, 261*, 32–39. https://doi.org/10.1016/j.jfoodeng.2019.04.022

Schreuders, F. K. G., Schlangen, M., Bodn, I., Erni, P., Boom, R. M., & Goot, A. J. Van Der (2022). Structure formation and non-linear rheology of blends of plant proteins with pectin and cellulose. *Food Hydrocolloids, 1*, 124. https://doi.org/10.1016/j.foodhyd.2021.107327, 107327.

Shand, P. J., Ya, H., Pietrasik, Z., & Wanasundara, P. K. J. P. D. (2007). Physicochemical and textural properties of heat-induced pea protein isolate gels. *Food Chemistry, 102*, 1119–1130. https://doi.org/10.1016/j.foodchem.2006.06.060

Sha, L., & Xiong, Y. L. (2020). Plant protein-based alternatives of reconstructed meat: Science, technology, and challenges. *Trends in Food Science & Technology, 102*(June), 51–61. https://doi.org/10.1016/j.tifs.2020.05.022

Sheikholeslami, Z., Karimi, M., Reza, H., & Mahfouzi, M. (2018). A new mixed bread formula with improved physicochemical properties by using hull-less barley flour at the presence of guar gum and ascorbic acid. *LWT - Food Science and Technology, 93*, 628–633. https://doi.org/10.1016/j.lwt.2018.04.001

Stiftung, Böll, H., & Terre, A. de la (2014). Meat atlas: Facts and figures about the animals we eat. *Heinrich Böll Foundation and Friends of the Earth Europe*. Retrieved from https://www.foeeurope.org/sites/def https://www.foeeurope.org/sites/default/files/publications/foee_hbf_meatatlas_jan2014.pdf. Retrieved from.

Stoica, A., Bărăscu, E., & Iuja, L. (2013). The influence of ascorbic acid and L-cysteine combination on bread quality. *Annals. Food Science and Technology, 14*(1), 50–53.

Strecker, T. D., Cavalieri, R. P., Zollars, R. L., & Pomeranz, Y. (1995). Polymerization and mechanical degradation kinetics of gluten and glutenin at extruder melt-section temperatures and shear rates. *Journal of Food Science, 60*(3), 532–537. https://doi.org/10.1111/j.1365-2621.1995.tb09820.x

Taghian Dinani, S., & Havet, M. (2015). Effect of voltage and air flow velocity of combined convective-electrohydrodynamic drying system on the physical properties of mushroom slices. *Industrial Crops and Products, 70*, 417–426. https://doi.org/10.1016/j.indcrop.2015.03.047

Takagi, H., & Ohtsu, I. (2017). *L-cysteine metabolism and fermentation in microorganisms in Amino Acid Fermentation*. Tokyo: Springer Japan. https://doi.org/10.1007/978-4-431-56520-8. Springer Japan.

Thrane, M., Paulsen, P. V., Orcutt, M. W., & Krieger, T. M. (2017). *Soy protein : Impacts , production , and applications. Sustainable protein sources*. Elsevier Inc. https://doi.org/10.1016/B978-0-12-802778-3.00002-0

Wang, Z., Tian, B., Boom, R., & van der Goot, A. J. (2019). Air bubbles in calcium caseinate fibrous material enhances anisotropy. *Food Hydrocolloids, 87*, 497–505. https://doi.org/10.1016/j.foodhyd.2018.08.037

Were, L., Hettiarachchy, N. S., & Coleman, M. (1999). Properties of cysteine-added soy protein – wheat gluten films. *Journal of Food Science, 64*(3), 514–518.

Wiedemann, C., Kumar, A., Lang, A., & Ohlenschläger, O. (2020). Cysteines and disulfide bonds as structure-forming units: Insights from different domains of life and the potential for characterization by NMR. *Frontiers of Chemistry, 8*, 280. https://doi.org/10.3389/fchem.2020.00280

Yang, N., Qian, S., Jiang, Z., & Hou, J. (2021). Cysteine inducing formation and reshuffling of disulfide bonds in cold-extruded whey protein molecules : From structural and functional characteristics to cytotoxicity. *Food Chemistry, 360*, Article 130121. https://doi.org/10.1016/j.foodchem.2021.130121

Yang, S., Zhang, Z., Li, J., Niu, Y., & Yu, L. L. (2021). Inhibition mechanism of L-cysteine on Maillard reaction by trapping 5-Hydroxymethylfurfural. *Foods, 10*(6), 1391. https://doi.org/10.3390/foods10061391

Zhang, Z., Elfalleh, W., He, S., Tang, M., Zhao, J., Wu, Z., et al. (2018). Heating and cysteine effect on physicochemical and flavor properties of soybean peptide Maillard reaction products. *International Journal of Biological Macromolecules, 120*, 2137–2146. https://doi.org/10.1016/j.ijbiomac.2018.09.082